ACS APPLIED NANO MATERIALS

www.acsanm.org Article

Fenton-Hydroxyl Radical Antioxidant Efficiency of Ibuprofen-Fe_3O_4-GO Nanospheres

Aleksey Drinevskyi, Evgenij Zelkovskyi, Vladimir Labunov, and Darya Radziuk*

Cite This: https://doi.org/10.1021/acsanm.3c05399 Read Online

ACCESS | Metrics & More | Article Recommendations | Supporting Information

ABSTRACT: A feasible one-step "solvent-antisolvent" oil-free acoustic emulsification method is demonstrated for the complexation of pristine ibuprofen with Fe_3O_4-GO in the form of nanospheres with a core−shell structure (~50 nm). The ultrasonic complexation occurs via the H-bond formation with the ibuprofen side chains (CH, CH_2, and CH_3) and C−O−H involving the interaction of carboxylic groups and Fe−O bonds. Synthesized ibuprofen-Fe_3O_4-GO nanospheres are efficient antioxidants with hydroxyl radical ($^{\cdot}OH$) scavenging and iron inactivation properties in the electro-Fenton process exhibiting ~24 times higher diminishing rate than free ibuprofen per se and ~161 times higher than pristine ibuprofen nanoparticles in aqueous medium. This pronounced antioxidant efficiency of ibuprofen-Fe_3O_4-GO nanospheres is due to the increased concentration of inactive protonated Fe(II) centers in Fe−O, C−Fe, and CO−Fe bonds (FeO^+, CFe^+, and $COFe^+$) of complexed drug molecules and increased concentration of CHO_2^+, OH^+, and CO^+ ions on the surface of nanospheres. The demonstrated method discloses the conditions of enhanced antioxidant efficiency of ibuprofen and defines the roles of Fe_3O_4 and GO in two basic fundamental COX-independent mechanisms.

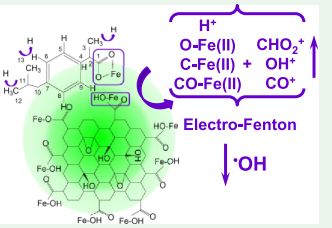

KEYWORDS: *graphene oxide, NSAID, iron oxide, ultrasound, metallodrug, Fenton, catalyst*

1. INTRODUCTION

Ibuprofen is one of the most useful nonsteroidal anti-inflammatory drugs (NSAIDs) available to humans to treat oxidant-mediated inflammatory diseases such as arthritis and musculoskeletal and rheumatic disorders.[1] Treatment of these diseases requires efficient molecules to attenuate reactive oxygen species (ROS) generation. The process of ROS formation is complex in cellular metabolic homeostasis and involves two defined mechanisms based on conversion of oxygen and hydrogen peroxide (H_2O_2) through the generation of ferrous ion Fe(II), impelling hydroxyl ($^{\cdot}OH$) radical production via Fenton reactions.[2] $^{\cdot}OH$ radicals can be also produced via Haber-Weiss reactions involving $O_2^{\cdot-}$ and H_2O_2.[3] Among ROS species, $^{\cdot}OH$ radicals are most destructive to cells because they cause the breakage of DNA strands, damage proteins, and lipids via peroxidation, induce mutagenesis or inhibit cancer suppressors.[4] As a result, intracellular free iron ions and highly reactive radical species can interact via the Fenton reaction, and interfere with the cell signaling processes, immunoregulation, and inflammation via induction of cytotoxicity.

Inhibition of intracellular ROS production such as O_2^- and H_2O_2 by ibuprofen has been reported.[5] Ibuprofen can scavenge the generated free oxygen radicals through the modification of low-density lipoproteins.[6,7] The ability of ibuprofen to suppress iron-mediated hydroxyl radical ($^{\cdot}OH$) generation from hydrogen peroxide (H_2O_2) was revealed in the Fenton reaction too.[8] Scavenging of $^{\cdot}OH$ radicals, i.e., free radical inactivation, may be one of the antioxidant mechanisms of ibuprofen in the treatment of rheumatic diseases.[9] In this way, in the electro-Fenton process ibuprofen exhibits a dual action: one that is related to the iron chelation, and the other one that involves the scavenging of $^{\cdot}OH$ radicals, leading to the production of reactive ibuprofen radicals that may be associated with the reported cytotoxicity of this drug.[10] Thus, ibuprofen can also act as a prooxidant as it is able to reduce Fe(III).[11] Therefore, the free radical inactivation by ibuprofen may be related either to hydrogen atom transfer via inactivation of free radicals through H donation or single electron transfer.

The antioxidant action of pristine ibuprofen was confirmed in the prevention of lung injury caused by oxidation and lipid peroxidation via chelation of iron, resulting in the formation of iron chelates that lack the free coordination site required for iron.[12] The antioxidant efficiency of ibuprofen is drug concentration-dependent: at a low concentration relative to that of iron, the drug acts as an efficient $^{\cdot}OH$ radical scavenger; at a higher concentration, excess of drug molecules inhibit the Fenton reaction and prevent H_2O_2 consumption by rendering iron nonreactive. Results show that the propionic acid group of ibuprofen can chelate iron, whereas its isobutylbenzene

Received: November 11, 2023
Revised: January 4, 2024
Accepted: January 5, 2024

https://doi.org/10.1021/acsanm.3c05399
ACS Appl. Nano Mater. XXXX, XXX, XXX−XXX

molecular part can contribute to the scavenging of ·OH radicals. Therefore, iron chelation may play a central role in ibuprofen's antioxidant mechanism of action and increase its biological function in analogy with the chelation activity of metals by organic substances, leading to selective cytotoxicity effects.[13]

The role of carboxylic groups in iron chelation by ibuprofen is crucial as it was evidenced that if the carboxylic acid group of ibuprofen was replaced by an ester, alcohol, amide, or tetrazole the anti-inflammatory activity of this drug was significantly reduced. Moreover, studies revealed that the antioxidant and antiradical activity of phenolic acids can be tightly linked to the number and position of −OH groups present on the aromatic ring. Therefore, the modification of pristine ibuprofen via metal complexation with its carboxylic group and aromatic C−C rings with its phenyl group could be a strategy to improve its antioxidant efficiency.

Modification of NSAIDs has been performed via metal ion complexation, e.g., mefenamic acid with Mn, Fe, Co, Ni, Cu, or Zn; diclofenac with Mn; indomethacin with Cu;[14] iron-salicylate complex[15] to produce antioxidant metallodrugs with ameliorated efficiency at the cellular level in comparison with pristine NSAIDs.[16] Previously, we have shown that complexation of pristine salicylic acid with Fe_3O_4-graphene oxide (GO) results in the formation of nanoparticles with intracellular switchable antioxidant function.[17] Magnetite nanoparticles (NPs) are biocompatible and exhibit negligible cytotoxicity, while GO provides a large surface active area, versatile chemistry, and enhanced stability of complexed molecules. Fe_3O_4-GO nanoplatform is regarded as a promising contrast agent for magnetic resonance imaging (MRI) and can significantly increase the loading capacity of organic molecules due to the $\pi-\pi$ stacking and hydrogen bonding.[18] From a biological point of view, Fe_3O_4-GO can increase ROS production, Ca^+ ion concentration, oxidative stress in mitochondria and activate Caspase-9 and Caspase-3 leading to cell apoptosis.[19] As Fe_3O_4-GO exhibits peroxidase-like activity, it can be potentially applied as a nanozyme.[20] At present Fe_3O_4-GO has been produced for loading with various drugs such as doxorubicin,[21] 5-fluorouracil,[22] camptothecin and methotrexate[23] and ultrasonic (20 kHz) functionalization of ketorolac[24] and acetylsalicylic acid (ASA).[25] Iron-based drugs are of special interest because Fe is a transition metal, which has multiple stable oxidation states and its redox chemistry can be accurately controlled.[26] However, only a few iron-based drugs (e.g., Proferdex, Dexferrum, InFeD, Venofer) are in clinical trials because the exact molecular mechanisms of their function and catalytic activity are not fully understood in the biological environment. Therefore, new methods of drug modification are needed to find conditions of metallodrug improved functionalization and efficiency.

Many methods have been introduced for metallodrug functionalization such as chemical metal-peptidic bioconjugation,[27] DNA G-quadruplex conjugation,[28] bioorthogonal synthetic lethality,[29] multiomics[30] and ultrasonic complexation via redox sonochemistry.[31] Sonochemistry can be related to one of the efficient tools to modify metallodrugs through the redox reactions of radical species, molecular assembly, and encapsulation mechanisms.[32−35] Up to now, sonochemistry has been applied to study sonofragmentation of pristine acetylsalicylic acid,[36] paracetamol, phenacetin, and sulfadimethoxine.[37] Another direction was to use a sonochemical emulsification tool for encapsulation of bioactive materials (paclitaxel, gemcitabine HCl, tetracycline, rifampicin, acetylsalicylic acid, a-tocopherol, piroxicam), RNA, Fe_3O_4 NPs in nanoscale carriers composed of cross-linked proteinaceous shells.[38] So far sonochemistry has been applied to synthesize stable Fe_3O_4 NPs;[39] to form Fe_3O_4-rGO[40] and graphene-dendrimeric Fe_3O_4 NPs for loading with doxorubicin and melatonin;[41] to encapsulate Fe_3O_4-GO and doxorubicin with folic acid conjugated chitosan;[42] to prepare Fe_3O_4@PEI-rGO for extraction of polar NSAIDs;[43] to use Fe_3O_4-GO for adsorption of bisphenol A, naproxen, and triclosan;[44] to form Fe_3O_4@C-nanodot@GO for the magnetic solid phase extraction of ibuprofen in human blood;[45] to load Fe_3O_4-GO with rapamycin;[46] and to use poly(2-aminobenzothiazole)-coated Fe_3O_4-GO for adsorption and extraction of naproxen, diclofenac, and ibuprofen.[47] Nowadays, little is known about the functionalization of pristine ibuprofen by sonochemistry to form catalytic ibuprofen-Fe_3O_4-GO with improved antioxidant function.

We introduce a feasible "solvent-antisolvent" oil-free acoustic emulsification method for the functionalization of pristine ibuprofen with Fe_3O_4-GO and determine the conditions of enhanced ·OH radical diminishing antioxidant activity of synthesized ibuprofen-Fe_3O_4-GO nanospheres. We show how this method enables efficient complexation of pristine ibuprofen with Fe_3O_4 and GO and explain why it can be useful in the fundamental understanding of ibuprofen-Fe(II), ibuprofen−Fe-O, and ibuprofen−C−O-Fe bonding in the study of COX-independent mechanisms of NSAIDs, inactivation of metal ions, and scavenging of free radicals.

2. EXPERIMENTAL SECTION

2.1. Materials and Synthesis. Pyrolytic graphite (mechanically ground by 3 mm balls for 70 min and thermally treated at $T = 100$ °C for 240 min) with composition C (95.9 ± 10.0) at %, O (3.7 ± 0.8) at %, and impurities of Ca (0.3 ± 0.1) at % was used for the synthesis of GO (more details can be found in Supporting Information). Potassium permanganate ($KMnO_4$, 99%), sulfuric acid (H_2SO_4, 93 wt %), phosphoric acid (H_3PO_4, 87 wt %), hydrogen peroxide (H_2O_2, 50 wt %), hydrogen chloride (HCl, 35 wt %), potassium hydroxide (KOH, 44 wt %), potassium chloride (KCl, 99.8%), sodium hydroxide (NaOH, 99%), disodium hydrogen phosphate ($Na_2HPO_4{\cdot}7H_2O$, 99%), citric acid (99%), isopropyl alcohol (C_3H_8O, 99.7%), ammonium hydroxide solution ($NH_3{\cdot}H_2O$, 25 wt %), and ethanol (C_2H_5OH, 96.2%) are of higher grade purity being obtained from Belreachim JSC (Republic of Belarus). Iron(II) chloride ($FeCl_2$, 98%) and iron(III) chloride ($FeCl_3$, 97%) were purchased from Sigma-Aldrich GmbH. Ibuprofen per se (99.5%) was obtained from IOL Chemicals and Pharmaceuticals Ltd. (India).

2.1.1. Synthesis of Ibuprofen-Fe_3O_4-GO Nanospheres. Ibuprofen-Fe_3O_4-GO nanospheres were synthesized by a "solvent-antisolvent" method with the use of an ultrasonic horn-type disperser with a diameter ~12 × 10^{-3} m of the irradiating surface and a maximal vibration amplitude 37 × 10^{-6} m operating in a continuous mode at 20 kHz frequency with the 400 W maximal output power (Cavitation Inc., Belarus). The stock solutions of pristine ibuprofen at concentrations 5 mM and 25 mM in ethanol (81 wt %) were used as "solvent" fluids. The aqueous solutions of GO, Fe_3O_4, and Fe_3O_4-GO were applied as "antisolvent" fluids to prepare ibuprofen-Fe_3O_4-GO nanospheres, ibuprofen-GO, and ibuprofen-Fe_3O_4 colloids for comparison studies.

Before the synthesis, a stock solution of GO (1 mg/mL) was prepared in deionized (DI) water by sonication at the intensity of ultrasound 24.54 ± 0.01 W/cm^2 for 165 min until the homogeneous suspension without a sediment was formed. A colloidal solution of Fe_3O_4 was prepared in DI water by using a coprecipitation method, in which iron is precipitated from the mixture of $FeCl_2$ and $FeCl_3$ at a

https://doi.org/10.1021/acsanm.3c05399
ACS Appl. Nano Mater. XXXX, XXX, XXX−XXX

molar ratio 1:2 in aqueous medium by addition of ammonium hydroxide solution in an argon atmosphere (more details in Supporting Information). The ultrasonic synthesis comprises the formation of Fe_3O_4-GO nanoplatform followed by its complexation with ibuprofen and ibuprofen-GO.

At first, preformed Fe_3O_4 NPs in a powder form (1 mg/mL) were dispersed in 10×10^{-3} L of an aqueous solution of GO (1 mg/mL) with ultrasound at intensity 16.36 ± 0.01 W/cm^2 for 60 min in an air atmosphere in an ice bath, resulting in the formation of Fe_3O_4-GO. Second, aqueous colloidal GO solution was dropwise added to 5 mM or 25 mM pristine ibuprofen solution (81 wt %) at the volume ratio 1:1 during ultrasonic treatment under mechanical stirring and sonicated at the intensity of ultrasound 24.54 ± 0.01 W/cm^2 for 1 min in an air atmosphere in the ice bath with the total volume of the reaction mixture 10×10^{-3} L. Pristine ibuprofen or the half of the ibuprofen-GO suspension ("solvent") was used for complexation with Fe_3O_4-GO ("antisolvent").

In a reaction of complexation, the "solvent" was sonicated at 24.54 $\pm$ 0.01 W/cm^2 while being dropwise added by an "antisolvent" at the volume ratio 1:1 and the reaction mixture was subjected to ultrasound for 3 min of total duration in an air atmosphere in ice bath to form ibuprofen-Fe_3O_4-GO nanospheres. Precipitation of obtained nanoparticles was carried out by centrifugation of the colloidal suspension at a relative centrifugal force of $9.5 \times g$ for 15 min in two cycles followed by removal of the supernatant. No white crystals of unreacted ibuprofen were observed. The obtained precipitant of final NPs was placed in the round-bottom glass vessel in a desiccator for thermal treatment at $T = 100 \pm 1$ °C for 5 h until a dry powder was formed.

Control experiments were performed following the abovementioned protocol of the synthesis in the absence of preformed GO or Fe_3O_4 or both of them to obtain ibuprofen-GO, ibuprofen-Fe_3O_4, and pure ibuprofen NPs. Each aqueous solution of GO and Fe_3O_4 was used as an "antisolvent" keeping the volume ratio of "solvent:antisolvent" as 1:1. For optical phase contrast microscope analysis, freshly prepared colloidal solutions were deposited on a glass coverslip via the drop-casting method and allowed for evaporation.

2.2. Equipment and Analytical Methods. The synthesized materials were characterized by using the following methods: transmission electron microscopy (TEM), scanning electron microscopy (SEM), energy dispersive X-ray fluorescence (EDX), X-ray powder diffraction (XRD), UV−visible absorbance spectroscopy, Fourier-transform infrared (FTIR) spectroscopy, and confocal Raman microscopy, time-of-flight secondary-ion mass spectrometry (TOF SIMS), and optical phase contrast microscopy.

The visualization of the inner and surface composition of prepared materials was performed by TEM (LEO-906E) Carl Zeiss, Germany. The morphology and elemental composition of synthesized products were characterized by SEM (S-4800) Hitachi, Japan. The phase composition, crystalline structure, and crystallite size of synthesized materials were determined by using powder diffraction patterns recorded with X-ray diffractometer Alrosa Group using Co Kα radiation at $\lambda = 1.79$ Å (Ni-filter) at 296 K with a scan step 0.005 and rate 0.1/min. Crystallite size t was determined by applying Scherrer's formula 1 to the most intensive plane (311) in the XRD pattern:

$$t = \frac{k\lambda}{\beta \cos \theta_B} \quad (1)$$

where k is the constant depending on the crystallite shape ($k = 0.89$ for GO and Fe_3O_4), λ is the X-ray wavelength (Co Kα = 1.79 Å), β is the integral breadth or full width at half-maximum, and θ_B is the Bragg angle. The most intense diffraction reflexes at $2\theta_B = 36.22°$ for Fe_3O_4 with $\beta = 0.325$ were used to calculate t values.

The electronic molecular properties of colloidal solutions were analyzed by UV−visible absorbance spectroscopy. The UV−visible absorbance spectra of colloidal solutions were recorded by using a PROSCAN spectrophotometer MC-122 (Belarus) operating with deuterium and halogen lamps in the wavelength ranges from 190 to 365 nm and from 330 to 1100 nm. For measurements, colloidal solutions were placed in a quartz (SUPRASIL) cuvette Hellma Analytics (Germany) 111-QS (Z600725) with a path length of 10 mm.

The identification of chemical groups and bonds present in synthesized nanoparticles was performed with the use of Fourier-transform infrared (FTIR) spectroscopy. FTIR spectra of synthesized powders were recorded by using a Bruker Alpha II FTIR spectrometer (USA) with a diamond crystal attenuated total internal reflectance (ATR) accessory. FTIR spectra were acquired in the wavenumber range from 4000 to 400 cm^{-1} (spectral resolution 2 cm^{-1}) by applying a suspension method of powders in KBr. A powder of synthesized materials was thoroughly ground with a dehydrated KBr at a weight ratio of 1:800 followed by pressing this mixture at ∼10 ton/mg into thin transparent spherical disks.

The surface molecular structure of synthesized materials was characterized by Raman spectroscopy. Raman spectra of colloids were recorded by using a laser 3D scanning confocal microscope Confotec NR500 (Belarusian-Japanese joint venture "SOLAR TII")) at 473 nm excitation wavelength with a grating 600 gr/mm blazed at 600 nm. The Si wafer with the characteristic Raman line at 520 cm^{-1} was taken as a reference for calibration and basic alignment during integration time from 3 to 50 s. The acquired Raman spectra were corrected for the baseline. A linearly polarized diode laser beam was focused through the objectives with 40× or 100× magnification for Raman spectra acquisition. The laser power was attenuated by using neutral density filters with the following OD values 0.6 (25), 0.3 (50), and no filter (100).

The elemental and molecular composition of nanoparticles was determined via acquisition of the mass/charge patterns in the use of a time-of-flight TOF.SIMS 5 secondary-ion mass spectrometer (IONTOF GmbH, Germany). For measurements, Si wafers were first purified by wet chemical cleaning method with the use of isopropanol, DI water, and ethanol. Second cleaned Si wafers were coated by a thin homogeneous layer of nanoparticles via the drop-casting procedure. SIMS measurements were performed by applying an Ar ion source in a static mode to keep the primary ion flux to a level that fragments a maximum of 1−10% of the coating surface with a spatial resolution ∼100 nm and a sampling depth of <2 nm.

2.2.1. Morphological Stability of Ibuprofen-Fe_3O_4-GO Nanospheres. The stability of prepared colloids and crystallization of ibuprofen were monitored by optical phase contrast microscopy via direct observation and recording by a high speed camera connected to an optical light microscope Planar MKI-2 M (Belarus) through taking photographs in real time and characterized by Software imaging tool ScopeTek Photo 3.1.312 (×86) of samples coated on glass coverslips. In experiments, the microscope objective was used with the aperture/focus 0.08/48 and the resolution 936 px in 0.1 mm.

2.2.2. Catalytic Activity of Ibuprofen-Fe_3O_4-GO Nanospheres. The electron-transfer reaction between 0.01 M $Fe(CN)_6^{3-}$ and 0.1 M $S_2O_3^{2-}$ at a volume ratio of 1:1 was chosen to examine the electrokinetic activity of 600 μL ibuprofen-Fe_3O_4-GO nanospheres in comparison with pristine ibuprofen. The absorbance spectra of aqueous colloidal solutions were measured with the use of a PROSCAN MC-122 spectrophotometer (Belarus) with an operating range from 190 to 1100 nm at a step 1 nm, wavelength setting accuracy: ± 0.2 nm and reproducibility ±0.1 nm at 25 ± 1 °C. The decline of the $Fe(CN)_6^{3-}$ peaks with and without nanoparticles was monitored by the absorbance at ≈420 nm as a function of time. The kinetics of the electron transfer during this reaction were examined every 5 min of reaction. Always freshly prepared hexacyanoferrate (III) and thiosulfate aqueous solutions were used in each kinetic run.

2.2.3. Electrochemical Measurements (the Electro-Fenton Process). The Fenton reaction, i.e., iron-catalyzed H_2O_2 decomposition, was chosen to examine the formation of OH and $^{\cdot}$OH radicals via the process of H_2O_2 decomposition catalyzed by iron cations Fe^{2+} at the contact with the synthesized colloids. In an experiment, 5 mM $FeCl_2$ (used as a catalyst) in DI water and 100 mM $Na_2HPO_4{\cdot}7H_2O$ (used as a phosphate-buffered solution, pH 9) in DI water were mixed at a volume ratio of 1:1. This mixture was added by H_2O_2 (50 wt %) at a volume ratio of 1:1:1.5 acidified by few drops of

https://doi.org/10.1021/acsanm.3c05399
ACS Appl. Nano Mater. XXXX, XXX, XXX−XXX

Scheme 1. Schematic Illustration Demonstrating the Principle of Ultrasonic Complexation (at 20 KHz) of Pristine Ibuprofen with Fe_3O_4-GO Nanoplatform via the Formation of Ibuprofen-Fe(II), Ibuprofen−Fe−O, and Ibuprofen−C−O−Fe Bonds in Ibuprofen-Fe_3O_4-GO Nanospheres with a Core−Shell Structure in the Frame of the Acoustic Emulsification Mechanism of a Biphasic "Solvent:Antisolvent" Mixture

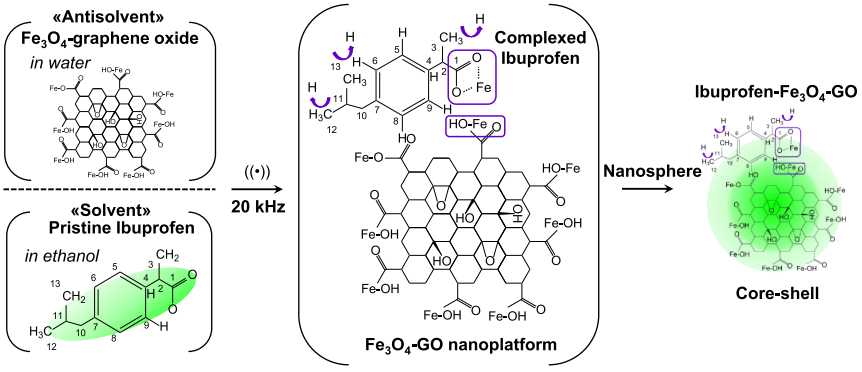

H_2SO_4 (93.6 wt %, pH 4.5) to perform the electro-Fenton process in a final volume of 35 mL in a glass vessel.

The Fenton reaction was carried out with the use of a three-electrode system consisting of working and counting electrodes as graphite paper sheets with the geometrical size 43 × 17 mm and a reference Ag/AgCl electrode. A stock 3.19 mol/L KCl aqueous solution was used as a supported electrolyte. Electrochemical measurements (cyclic voltammetry) were performed with the Metrohm Autolab potentiostat/galvanostat instrument operating with the Nova 1.11 software allowing data acquisition and analysis.

Electrochemical experiments were carried out by adding 1×10^{-3} L of free ibuprofen (in ethanol solution) or synthesized nanospheres in aqueous solution in the total volume of 5×10^{-3} L during the electrochemical process of 10 scans at scan rate 0.1 V/s in the applied voltage range from −0.5 to +1.2 V.

3. RESULTS AND DISCUSSION

In this work, we demonstrate the principle of functionalization of pristine ibuprofen via ultrasonic complexation at the contact with Fe_3O_4-GO nanoplatform through the formation of ibuprofen-Fe(II), ibuprofen−Fe−O and ibuprofen−C−O−Fe bonds by applying the "solvent:antisolvent" precipitation technique. Acoustic emulsification is used as a tool for a biphasic mixture consisting of pristine ibuprofen in ethanol solution ("solvent") and aqueous colloidal Fe_3O_4-GO solution ("antisolvent") to prepare ibuprofen-Fe_3O_4-GO nanospheres with a core−shell structure as shown in Scheme 1.

The ultrasonic complexation of pristine ibuprofen takes place at the ethanol:water interface under ultrasound (20 kHz) that induces emulsification of two fluids "solvent:antisolvent" in a single-step procedure. Our method of ultrasonic complexation is based on the acoustic emulsification of a biphasic mixture consisting of a "solvent" as a nonpolar liquid and an "antisolvent" as a polar liquid. The main parameters of fluids in this process are the density ρ and viscosity η of liquids, and speed υ of sound in these liquids, while the volume fraction and the order of addition of one liquid into the other along with the acoustic pressure amplitude will determine the final size of obtained droplets according to a two-step mechanism of acoustic emulsification proposed by H.S. Folger and his colleagues in 1978. In this way, the first stage of acoustic emulsification is the formation of large droplets by the rupture of waves on a planar "solvent:antisolvent" interface. In the second stage, the large droplets are continually broken into smaller droplets by the shock waves emanating from the collapse of cavitation bubbles.

In our experiments, the density of "antisolvent" (density of magnetite ∼5170 kg/m^3 and water ∼1000 kg/m^3 at T = 20 °C) is larger than the density of "solvent" (density of ethanol ∼789 kg/m^3 at T = 20 °C and ibuprofen at 5 mM ∼1.0 kg/m^3 and at 25 mM ∼5.2 kg/m^3 at T = 20 °C). As the density of "solvent" is relatively low, the intensity of ultrasound is higher in it than in "antisolvent" which is determined by the following equation $I = P_A^2/2\rho\upsilon$, where P_A is the maximum pressure amplitude, ρ is the density of a liquid, and υ is the speed of sound in this liquid. We can consider the kinematic viscosity, which is defined as $\eta = \mu/\rho$, where μ is the dynamic viscosity and ρ is the density of the fluid, the ratio of viscosity magnitudes of "solvent" to "antisolvent", i.e., η_{sol}:$\eta_{antisol}$ is ∼7.8. Therefore, the propagation of sound waves in "solvent" is easier and faster because of the higher intensity of ultrasound in contrast to the "antisolvent" phase, which acts rather as an acoustic impedance at 20 kHz and constant acoustic pressure amplitude.

Taking into consideration all these parameters of two liquid phases: "solvent" and "antisolvent", we can define the approximate size of initial large particles as of ∼37 μm because of the amplitude of the irradiating and vibrating horn, which determines the disruption of the planar interface formed between these two phases according to the type of Rayleigh−Taylor instability mechanism. By definition, the Rayleigh−Taylor instability mechanism occurs between two fluids of different densities, when the lighter fluid is pushing the heavier one. In our case, the solvent is pushing the antisolvent by the Rayleigh−Taylor instability mechanism. The equilibrium of this biphasic "solvent:antisolvent" mixture is unstable to any perturbations or disturbances of the interface, which has a lower potential energy in comparison with the initial state of the two fluids. In this way, the more dense "antisolvent" phase is dispersed into the less dense and more viscous "solvent" phase, which basically should coat the surface of "antisolvent" drops in the biphasic mixture. As a result of it, ibuprofen-Fe_3O_4-GO nanospheres with a distinct core−shell structure can be formed.

It is more probable that such a core−shell structure is formed at the first step of acoustic emulsification. The short duration of sonication (3 min) is sufficient for the drops (particles) to break up into very small particles, which is determined rather by the density and viscosity magnitudes of fluids and a high intensity of applied acoustic field. One more argument, the higher hydrophobicity of the "solvent" phase

https://doi.org/10.1021/acsanm.3c05399
ACS Appl. Nano Mater. XXXX, XXX, XXX−XXX

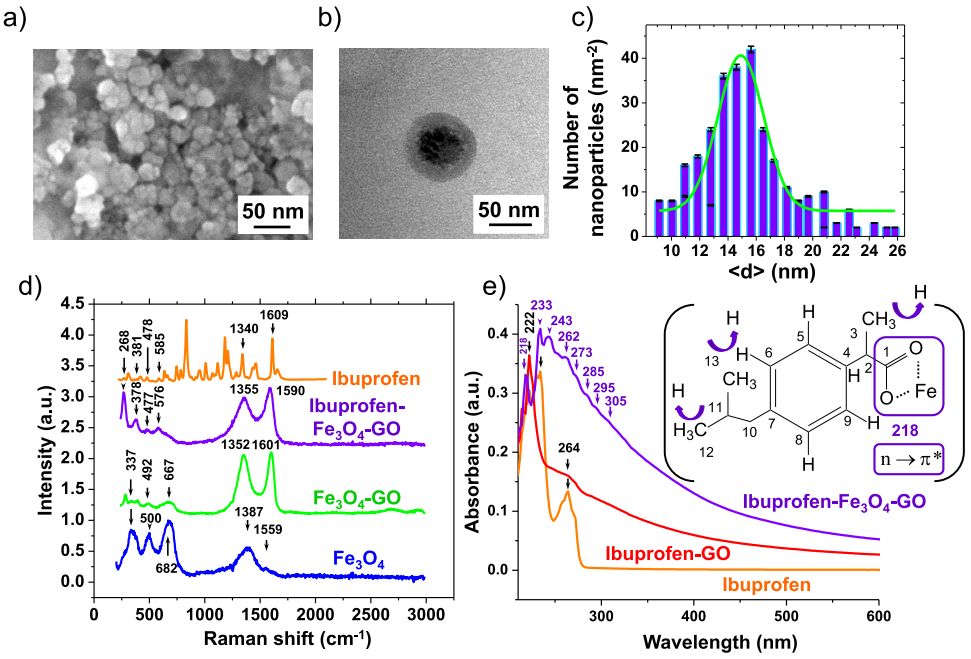

Figure 1. Representative (a) SEM and (b) TEM images of synthesized ibuprofen-Fe_3O_4-GO nanospheres are shown with (c) statistical diagram of the average size distribution of dark particulates per surface area (nm^2) that form larger assemblies. (d) Raman spectra of ibuprofen-Fe_3O_4-GO and Fe_3O_4 NPs, Fe_3O_4-GO nanoplatform, and pristine ibuprofen are shown (λ_{exc}= 473 nm). (e) UV−vis absorbance spectra of aqueous colloidal solutions of ibuprofen-Fe_3O_4-GO and ibuprofen-GO and free ibuprofen per se (81 wt %) are demonstrated. The inset scheme shows the changes of the ibuprofen molecular structure according to the observed characteristic absorbance bands indicating hydrogen atom abstraction, modified phenyl ring, and complexation of the carboxyl group with Fe (at 218 nm).

may lead ibuprofen and ethanol molecules to be adsorbed at the cavitation interface being able to penetrate the hot gaseous bubble interior upon implosive collapse and directly experience the shock waves emanatig to the distance of ∼200 nm from the center of the hot spot. This scenario is realistic according to the nanodroplet injection model of cavitation bubbles, which was experimentally proved by the group of Prof. K.S. Suslick.

Let us examine the electronic-molecular properties of ibuprofen-Fe_3O_4-GO nanospheres through the study of individual components such as GO and Fe_3O_4 at the contact with ibuprofen in comparison with pristine drug molecules to understand the ultrasonic complexation mechanism.

3.1. Ultrasonic Complexation of Ibuprofen with the Fe_3O_4-GO Nanoplatform. At first, we synthesized small GO colloids with a uniform structure by applying the second oxidation procedure according to the improved Hummers protocol (more details in Supporting Information). Prepared GO material has a C/O ratio ∼1.49, which is lower than that of GO from the first oxidation step (∼1.83), indicating enhanced oxidation of graphene sheets and formation of oxygen functional groups (Figure S1). This GO was used for the synthesis of Fe_3O_4-GO nanoplatform, which appeared in the form of nonuniform spheres of average size (26.9 ± 7.1) nm with a thin layer coating of the following elemental composition (at %): O (48.1 ± 2.7), Fe (43.1 ± 2.1), C (8.6 ± 0.6) (incl. Cl ∼0.14) and C/O ratio of ∼0.18 (Figure S2).

Acoustic emulsification of a biphasic mixture consisting of ethanolic solution of pristine ibuprofen ("solvent") and aqueous colloidal solution of Fe_3O_4-GO nanoplatform ("antisolvent") leads to the formation of final ibuprofen-Fe_3O_4-GO nanoparticles with a spherical shape and a distinct core−shell structure (Figure 1a,b). The core of final ibuprofen-Fe_3O_4-GO nanoparticles consists of small dark particulates with an average size 14.91 ± 0.17 nm that form an assembly of a larger size ∼50.81 ± 0.23 nm (Figure 1c). This dark core is coated by a gray shell with a thickness ∼14.0 nm. Careful study of TEM images of these nanoparticles revealed their porous inner structure with two distinct regions: a black core and a gray shell in contrast to produced pristine ibuprofen NPs (Figure S3).

3.2. Surface Molecular Composition of Ibuprofen-Fe_3O_4-GO. The surface molecular composition of formed ibuprofen-Fe_3O_4-GO nanospheres was determined by Raman spectroscopy via comparison with Raman spectra of free ibuprofen per se, Fe_3O_4, and Fe_3O_4-GO NPs (Figure 1d). Raman spectra of ibuprofen-Fe_3O_4-GO nanospheres show a characteristic peak of iron oxide with the magnetite phase at 576 cm^{-1},[48] D band at ∼1355 cm^{-1} caused by amorphization and oxidation of graphitic nanocrystals[49] and the G band at ∼1590 cm^{-1} of GO with sp^2-bonded carbon atoms consisting of distorted 6-fold rings or rings of other orders,[50] and peaks of ibuprofen at 268, 378, and 477 cm^{-1},[51,52] which confirms the formation of magnetite-graphene structure in the complex with ibuprofen.

Raman spectra of the Fe_3O_4-GO nanoplatform reveal the band of Fe_3O_4 at ∼337 cm^{-1}, and vibrations of Fe−O (∼492 cm^{-1}) and Fe_3O_4 (∼667 cm^{-1}),[53] indicating the formation of Fe_3O_4 NPs on the surface of GO. The intensity ratio of D and G bands Int(D)/Int(G) is ∼0.83 in ibuprofen-Fe_3O_4-GO nanospheres and ∼0.95 in Fe_3O_4-GO nanoplatform, indicating the lower density of defects in nanospheres.

For comparison, Raman spectra of Fe_3O_4 NPs stabilized with citric acid ligands reveal the iron oxide phase with an organic coating by citrate ligands caused by laser-induced oxidation (∼337 cm^{-1})[53] and demonstrate the formation of Fe−O−Fe (∼500 cm^{-1})[54] bonds and Fe_3O_4 (∼682 cm^{-1})

https://doi.org/10.1021/acsanm.3c05399
ACS Appl. Nano Mater. XXXX, XXX, XXX−XXX

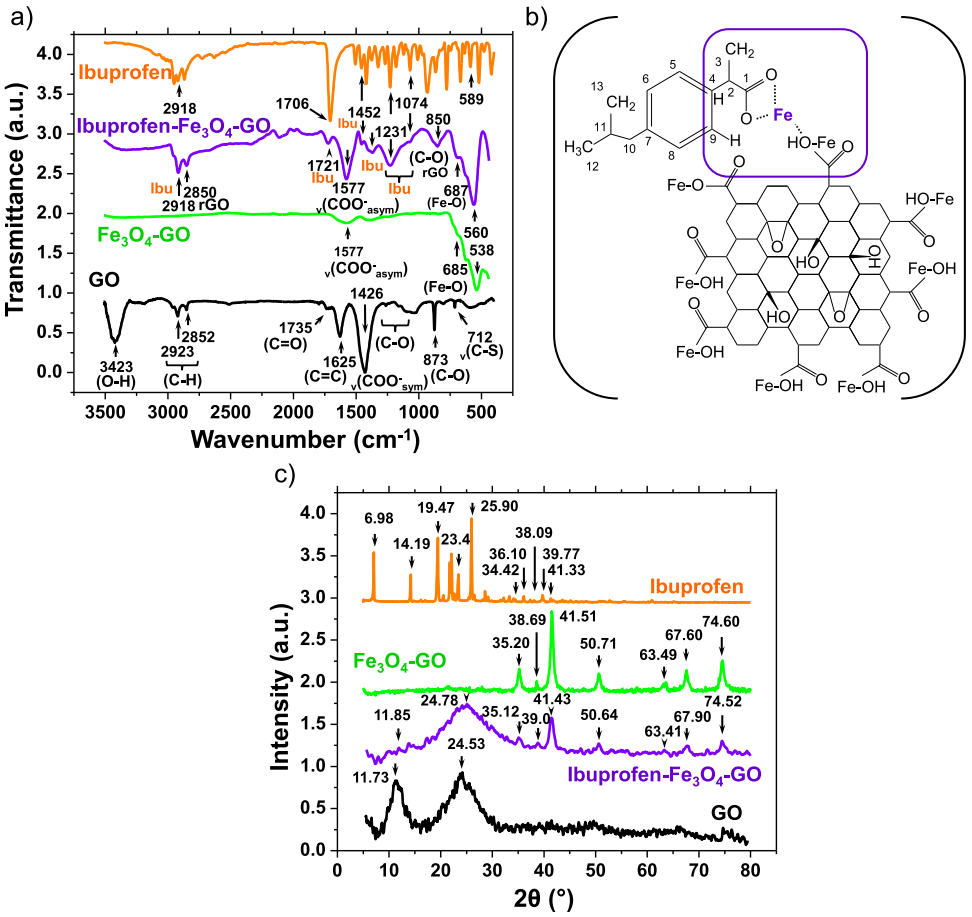

Figure 2. (a) Fourier-transform infrared transmittance spectra of ibuprofen-Fe_3O_4-GO, Fe_3O_4-GO and GO nanoparticles in comparison with ibuprofen per se are shown. (b) Schematic illustration shows a chemical structure of ibuprofen-Fe_3O_4-GO nanospheres indicating the formation of Fe−O and Fe−OH bonds between ibuprofen and GO with the magnetite phase. (c) X-ray powder diffraction patterns of ibuprofen-Fe_3O_4-GO nanospheres are shown in comparison with Fe_3O_4-GO nanoplatform, GO and ibuprofen per se.

phase.[55] Vibrational modes at ∼1387 and ∼1559 cm^{-1} can be assigned to the magnetite phase at the nanoscale with the surface coated by citrate ligands under oxidation induced by laser excitation[56] as compared with the reference of Raman spectrum of bulk magnetite (Figure S4).

3.3. Electronic Molecular Structure of Ibuprofen-Fe_3O_4-GO Nanospheres. The electronic molecular structure of ibuprofen-Fe_3O_4-GO nanospheres was assessed by UV−vis absorbance spectroscopy (Figure 1e). The UV−vis absorbance spectrum of an aqueous solution of these nanospheres is manifold with one distinct peak at ∼218 nm and the series of smaller peaks at ∼233, 243, 262, 273, 285, 295, and 305 nm on an elevated continuum, indicating complex electronic ibuprofen-Fe_3O_4-GO structure, in which the chromophore of ibuprofen can be located within the surface layers of nanospheres. To understand this complexity of nanospheres, let us refer to the pristine ibuprofen (absolute ethanol solution, pH 5.5), which absorbs light at ∼222, 233, and 264 nm as a result of the electronic $\pi-\pi^*$ transitions of its modified phenyl group and the electronic transitions of ibuprofen $\pi_{PY} \rightarrow \pi_{CO^*}$ occurring between the phenyl ring and C−O bonds caused by oxidation of hydroxyl radicals.[57]

Ultrasonic complexation of ibuprofen with GO leads to the enhancement of absorbance at ∼222 nm and disappearance of band at ∼233 nm, indicating the decreased concentration of protonated species, which exhibit the first vertical S1 excitation (HUMO→LUMO) of $\pi-\pi^*$ nature.[58] In an aqueous solution of ibuprofen-GO NPs (50 wt %, pH 5.5) the strong band at ∼264 nm becomes broad with much lower intensity than in pristine ibuprofen, which is indicative for the substitution in the side chains of the drug molecular structure within the modified phenyl ring.[59]

Therefore, ultrasonic complexation of pristine ibuprofen with Fe_3O_4-GO nanoplatform involves abstraction of a hydrogen atom by ·OH radicals forming the methylbenzyl[57] and other benzyl type and hydroxycyclohexadienyl type radicals due to $\pi-\pi^*$ transitions. The bathochromic shift of a band in ibuprofen-Fe_3O_4-GO nanospheres in high energy region from 210 to 215 to 218 nm indicates the formation of a complex between Fe and carboxyl group of ibuprofen due to $n-\pi^*$ transitions, which can be caused by the charge transfer reaction between the drug ligands and iron atoms in Fe_3O_4-GO or due to the formation of ion-pair complexes. The appearance of a small band at ∼243 nm is caused by the shift of a band at ∼264 to ∼262 nm accompanied by the appearance of multiple smaller peaks up to 305 nm, demonstrating that hydroxylation may take place in the side chains and also in the ring of ibuprofen as a result of reaction with ·OH radicals.[59] The absorbance band of ibuprofen-Fe_3O_4-GO nanospheres at ∼273 nm is caused by the interaction of ibuprofen with ethanol. The relatively low intensity of a band at ∼285 nm points out to the domination of the hydroxycyclohexadienyl

https://doi.org/10.1021/acsanm.3c05399
ACS Appl. Nano Mater. XXXX, XXX, XXX−XXX

Table 1. Analysis of Experimental X-ray Powder Diffraction 2θ (deg) Values Is Shown with Calculated Interplanar Spacing d (nm) Magnitudes of GO, Fe_3O_4-GO Nanoplatform, and Ibuprofen-Fe_3O_4-GO Nanospheres (Co K_α = 1.79 Å)

material	2θ (deg)	int. (a.u.)	d (nm)	(hkl)	assignment
GO	11.73	100	0.876	(001)	GO
	24.53	82	0.421	(003)	GO
ibuprofen-Fe_3O_4-GO	11.85	1	0.866	(001)	GO
	24.78	100	0.417	(003)	GO
	35.12	67	0.297	(220)	Fe_3O_4
	39.00	61	0.268	(004)	GO
	41.43	86	0.253	(311)	Fe_3O_4
	50.64	59	0.209	(400)	Fe_3O_4
	63.41	52	0.170	(422)	Fe_3O_4*
	67.90	58	0.160	(511)	Fe_3O_4*
	74.52	61	0.148	(440)	Fe_3O_4
Fe_3O_4-GO	35.20	44	0.296	(220)	Fe_3O_4
	38.69	33	0.270	(004)	GO
	41.51	100	0.253	(311)	Fe_3O_4
	50.71	41	0.209	(400)	Fe_3O_4
	63.49	36	0.170	(422)	Fe_3O_4
	67.60	48	0.161	(511)	Fe_3O_4
	74.60	58	0.148	(440)	Fe_3O_4

type radicals and formation of hydroxylated products in the ring. Therefore, it can be concluded that the carboxyl group of ibuprofen, which is directly involved in the complex formation with iron, and the oxidized form of the phenyl group contribute to the increase of the electron density of ibuprofen within the Fe_3O_4-GO nanoplatform.

3.4. Chemical Bond Formation between Ibuprofen, Fe_3O_4, and GO. Next, ibuprofen-Fe_3O_4-GO nanospheres were characterized by the use of FTIR spectroscopy to understand the chemical bond formation between ibuprofen, Fe_3O_4, and GO (Figure 2a). The analysis of bands from FTIR transmittance spectra of pristine ibuprofen (Table S1), GO, Fe_3O_4-GO, and ibuprofen-Fe_3O_4-GO nanospheres are shown in Tables S2−S4 (Supporting Information). FTIR spectrum of GO shows characteristic modes of $_\nu$(C−S) (~712 cm^{-1}), C−O vibrations of epoxide groups (~873 cm^{-1}, 1021−1220 cm^{-1}), $_\nu$(COO^-) and C═O of carboxyl and carbonyl groups (~1426 cm^{-1}, 1735 cm^{-1}), deformation of water molecules intercalated in oxidized graphitic domains (~1625 cm^{-1}), aliphatic C−H stretching (2852 and 2923 cm^{-1}) and adsorbed water molecules, hydroxyl and carboxyl groups (~3190 and 3423 cm^{-1}) (Table S2). Therefore, synthesized GO consists of hydroxyl, carboxyl, and epoxide groups with the presence of large aromatic regions and is free of bisulfate, O_3S−OH, O═S═O, $-SO_3$, and H_3O^+ groups, which is indicative for high-purity GO nanosheets.[60] FTIR spectra of Fe_3O_4-GO nanoplatform show a distinct band at ~538 cm^{-1} and two shoulders near ~624 and 685 cm^{-1}, which can be assigned to Fe_3O_4 after oxidation caused by either elevated temperature[61] or by the interaction with GO according to the proposed dynamic structural model with migrating oxygen functional groups[62,63] (Table S3).

In ibuprofen-Fe_3O_4-GO, the fundamental Fe−O vibration is upshifted from 538 to 560 cm^{-1} and develops a shoulder at 687 cm^{-1}, which is indicative for Fe_3O_4 with adsorbed hydroxyl groups caused by oxidation at the contact with GO and ibuprofen during acoustic emulsification (Table S4). The vibrational displacement of oxygen atoms in C−O of GO (according to the dynamic structural model) confirms the enhanced oxidation of the NPs surface.

In ibuprofen-Fe_3O_4-GO nanospheres, ibuprofen exhibits C−H bending, CH_2 twisting, and CH_3 rocking at ~1074 cm^{-1}, CO−H in-plane bending (H-bonded) at ~1231 cm^{-1}, C−H bending, C−C−O stretching and CO-H bending at ~1370 cm^{-1}, ring vibration and CH_3 antisymmetric deformation at ~1452 cm^{-1} and C═O stretching (H-bonded) at ~1721 cm^{-1}, CH_3 out of phase symmetric stretching at ~2918 cm^{-1}, pointing out to the specific complexation of drug ligands through the H-bond formation with Fe_3O_4-GO nanoplatform. The observed $_\nu$(COO^-) asymmetric stretch of the carboxyl group at ~1577 cm^{-1} in Fe_3O_4-GO is strongly enhanced in ibuprofen-Fe_3O_4-GO nanospheres, confirming the complexation of ibuprofen with nanoplatform (Figure 2b). Therefore, one may conclude that the side chains of ibuprofen such as CH, CH_2, and CH_3 can form H-bonds with C−O−H and involve the interaction of carboxylic groups with Fe−O bonds in Fe_3O_4-GO nanoplatform bearing surface adsorbed OH groups.

3.5. Crystalline Structure of Ibuprofen-Fe_3O_4-GO. The crystalline structure of ibuprofen-Fe_3O_4-GO nanospheres was examined by X-ray powder diffraction in comparison with patterns of pristine ibuprofen (Table S5), GO and Fe_3O_4-GO nanoplatform (Figure 2c and Table 1). The XRD pattern of GO in a solvent-free state shows two distinct reflexes at 2θ = 11.73° and 24.53° with the interplanar spacing values ~8.759 and ~4.215 Å, which can be assigned to (001) and (003) of GO.[64] The interplanar spacing of the (001) plane is 0.779 Å higher than in graphite intercalation compound (~7.980 Å) during the process of GO formation, which is indicative of the intercalation of oxygen atoms in the forming oxidized domains. On the other hand, the d ~8.759 Å of (001) is comparable to the lattice expansion of (001) in GO caused by intercalation of 1-propanol (~8.650 Å). The 2θ peak at ~24.53° indicates the heterogeneous nature of GO that contains carbon domains with sp^2- and sp^3 hybridization. The crystallite size of synthesized GO is ~7.41 Å (2θ = 24.53°, β = 0.22), which corresponds to ≈2 layers of graphene assuming the van der Waals diameter of carbon ~3.45 Å.[64]

The interplanar spacing values of ibuprofen-Fe_3O_4-GO nanospheres are comparable with the Fe_3O_4-GO nanoplatform

https://doi.org/10.1021/acsanm.3c05399
ACS Appl. Nano Mater. XXXX, XXX, XXX−XXX

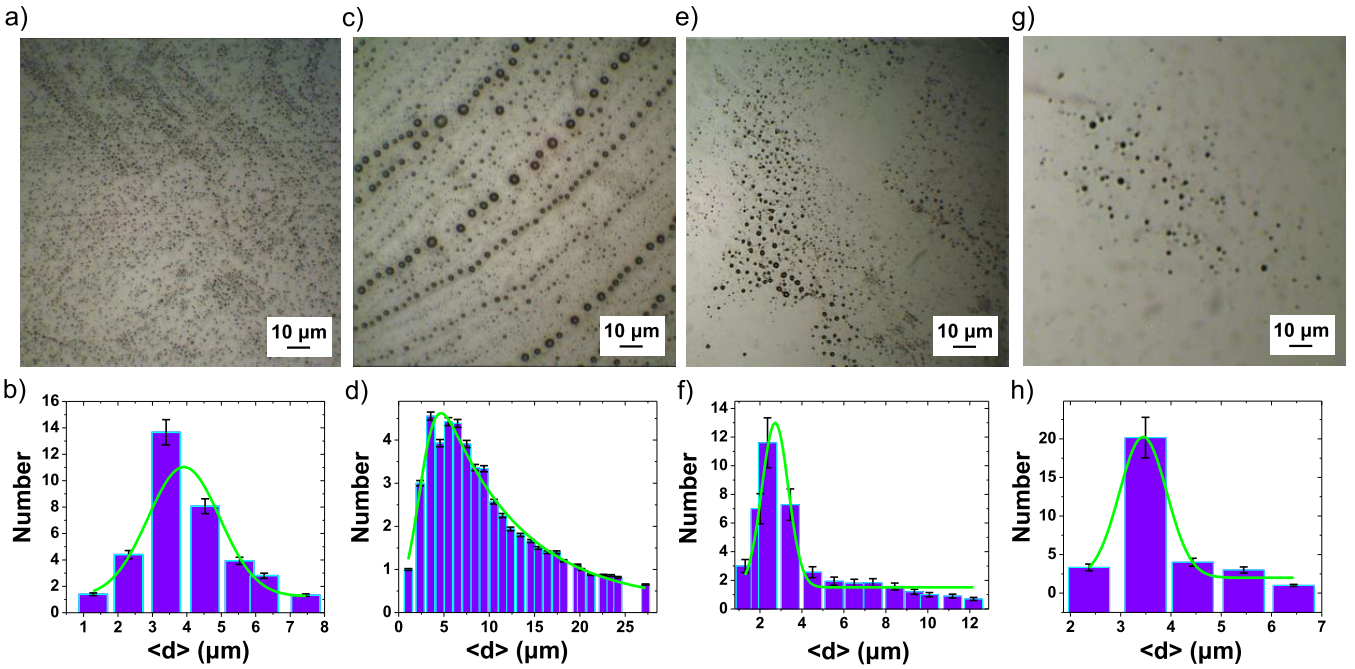

Figure 3. Optical phase contrast microscopy images of pristine ibuprofen spheres and their average diameter distribution histograms before (a,b) and after 24 h of aging (c,d); ibuprofen-Fe_3O_4-GO spheres before (e,f) and after of 24 h of aging (g,h) are shown (scale bar is 10 μm). The initial concentration of ibuprofen per se in all experiments was 25 mmol/L.

revealing GO, and the phases of graphite-diamond intermediate and magnetite (Table 1), but not of ibuprofen per se.[65] The XRD reflexes of ibuprofen per se can be assigned to the crystalline structure of rac-ibuprofen form II in a hydrated state[66] (Table S5). The XRD pattern of the Fe_3O_4-GO nanoplatform shows characteristic reflexes of GO and Fe_3O_4 obtained at ~1.55 GPa.[67] In the XRD pattern of ibuprofen-Fe_3O_4-GO nanospheres, most of the reflexes indicate pure magnetite phase[24] except the interplanar spacing values of (422) and (511), which are decreased and can be assigned to the high-pressure effect of ~4.99 GPa on Fe_3O_4*.[68] Such high pressure can cause the reduction of the interplanar spacing values of GO from 0.876 to 0.866 nm, from 0.421 to 0.417 nm, and graphite-diamond intermediate from 0.270 to 0.268 nm. Under such conditions, the H-ordering in carboxylic acids can be affected by increasing the intermolecular interactions involving the carboxyl oxygen atoms and by compressing the O···O distances, resulting in a decrease of the potential-energy barrier between the H-sites, facilitating the H-disordering.[69]

3.6. Colloidal Stability of Ibuprofen-Fe_3O_4-GO Nanospheres. The colloidal stability of ibuprofen-Fe_3O_4-GO nanospheres was examined by optical phase contrast microscopy (Figure 3). Microscopic images reveal monodisperse spherical pristine ibuprofen NPs with an average diameter $\langle d \rangle = (2.90 \pm 0.07)$ μm that form a uniform coating on the glass coverslip (Figure 3a,b).

After 24 h of aging in a mother solution, the average diameter of these NPs became smaller $< d \geq (2.41 \pm 0.21)$ μm, and its distribution histogram became broader demonstrating an increased amount of NPs with larger diameters up to ~20 μm (Figure 3c,d). Therefore, one may assume that after 24 h NPs increased their diameter including the minority of smaller NPs with the initial <d> less than ~2.9 μm. In contrast, the average diameter of ibuprofen-Fe_3O_4-GO nanospheres <d> = (2.72 ± 0.04) μm (Figure 3e,f) increased up to 3.45 ± 0.04 μm (Figure 3g,h) and the largest detected diameter of spheres did not exceed ~8 μm. All types of NPs preserved their spherical shape. In this way, complexation of ibuprofen with Fe_3O_4-GO nanoplatform significantly slows down the growth of spheres in comparison with pristine ibuprofen NPs.

3.7. Catalytic Activity of Ibuprofen-Fe_3O_4-GO Nanospheres. The catalytic activity in the inhibition of $^{\cdot}OH$ radical formation on the surface of ibuprofen-Fe_3O_4-GO nanospheres was examined in comparison with ibuprofen per se (81 wt %) and pristine ibuprofen NPs in the electro-Fenton process (Figure 4). The formation of $^{\cdot}OH$ radical is associated with the characteristic current peaks at ~4.86 mA (~0.45 V) due to oxidation and at ~−4.66 mA (~0.15 V) due to reduction, indicating the reversible electro-Fenton process (Figure 4a). Soon after the introduction of ibuprofen-Fe_3O_4-GO nanospheres in the Fenton reaction system, current peaks diminished in a concentration-dependent manner of complexed ibuprofen. In particular, the oxidation peak of $^{\cdot}OH$ radicals disappeared at a rate ~of 2.7×10^3, when the concentration of ibuprofen in ibuprofen-Fe_3O_4-GO nanospheres increased from 41.15 to 205.75 μg/mL, demonstrating the radical scavenging ability of complexed ibuprofen (Figure 4b). In a reversible redox cycle the current reduction peak also disappeared, indicating that the contribution of reaction products such as H^+, O_2, and H_2O molecules became less.

The cyclic voltammograms reveal that no oxidation of ibuprofen occurred because the characteristic oxidation peak at ~+1.2 ± 0.2 V did not appear, meaning that no transfer of an electron takes place and no radical-cation (in oxidation) or radical-anion (in reduction) of ibuprofen is formed as a result of a decarboxylation process.[70] In this way, the scavenging efficiency of either complexed or free ibuprofen molecules is not associated with the reported toxicity of ibuprofen.

The decrease of current peaks in the electro-Fenton process was observed in the reaction systems containing free ibuprofen per se (Figure 4c) or pristine ibuprofen NPs (Figure 4e) but at

https://doi.org/10.1021/acsanm.3c05399
ACS Appl. Nano Mater. XXXX, XXX, XXX−XXX

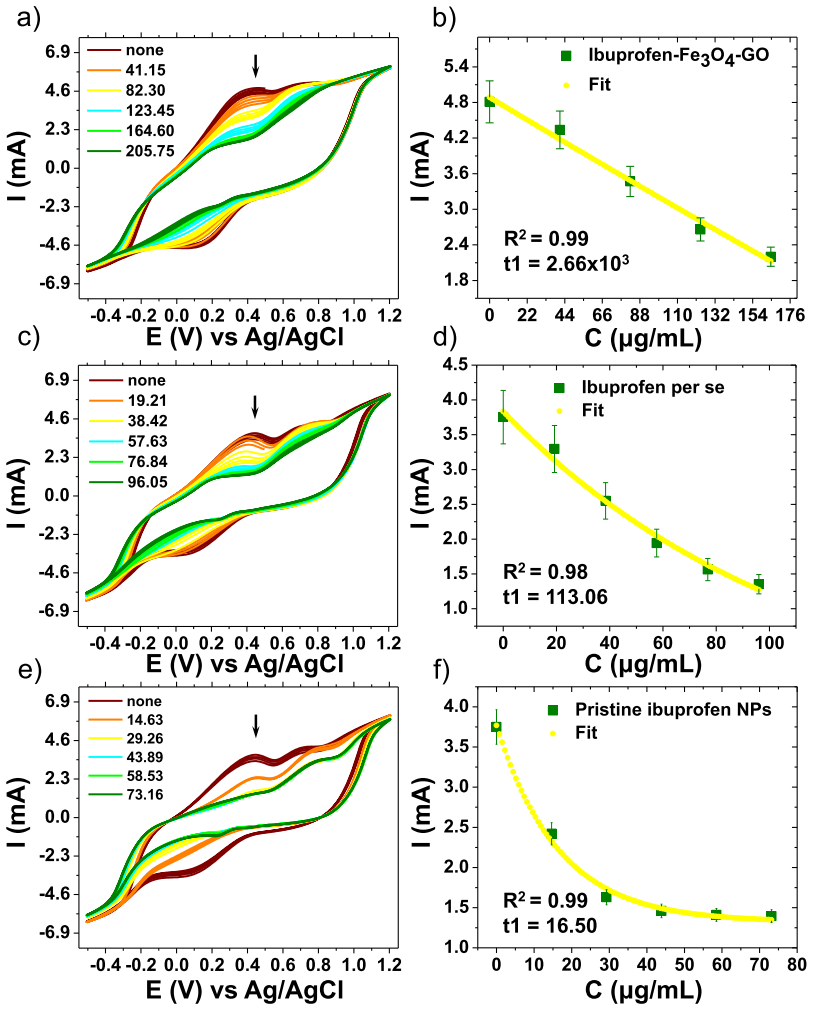

Figure 4. Cyclic voltammograms show the relative response of current I (mA) in aqueous solutions of (a,b) ibuprofen-Fe_3O_4-GO in the concentration range of complexed ibuprofen from 41.15 to 205.75 μg/mL, (c,d) ibuprofen per se (81 wt %, from 19.21 to 96.05 μg/mL), and (e,f) pristine ibuprofen NPs (from 14.63 to 73.16 μg/mL) in an applied potential range from −0.5 to +1.2 V and the plots demonstrating the decay of corresponding current peak values of $^{\cdot}$OH formation versus concentration as indicated by a black arrow.

slower decay rates ∼113.0 (Figure 4d) and ∼16.5 (Figure 4f). In this way, the inhibition of $^{\cdot}$OH radicals by ibuprofen-Fe_3O_4-GO nanospheres is ∼23.5 times higher than of free ibuprofen per se and ∼161.2 times higher than of pristine ibuprofen NPs. In general, the electrochemical oxidation of pristine ibuprofen corresponds to the electrochemical-chemical mechanism involving the transfer of an electron followed by a homogeneous chemical reaction. The mechanism of the electrochemical oxidation of ibuprofen is not pH-dependent and possibly involves a single electron transfer via radical cation formation, followed by decarboxylation. The decreased radical scavenging efficiency of noncomplexed ibuprofen may be associated with the drug's action as a prooxidant as it is able to reduce Fe(III).[16] On the other hand, ibuprofen can form iron chelates that lack the free coordination site required for iron.[12] However, in contrast to its noncomplexed state, complexed ibuprofen in Fe_3O_4-GO nanospheres can contain chelated iron, thereby providing additional catalytic sites for the more efficient inhibition of Fenton oxidation process.

3.8. Antioxidant Mechanism of Ibuprofen-Fe_3O_4-GO.

From the literature, a chelate, which contains a free coordination site and allows iron reactivity, readily combines with a substance at a free coordination site, causing a spectral shift. In contrast, a chelate with a compound that decreases iron reactivity leaves no coordination site open and shows no spectral shift. To test the idea of iron chelation by ibuprofen, we studied the electron transfer reaction between $Fe(CN)_6^{3-}$ and $S_2O_3^{2-}$ at the contact with ibuprofen-Fe_3O_4-GO (4.9 μg/mL of complexed ibuprofen) and pristine ibuprofen NPs (8.8 μg/mL of complexed ibuprofen) and monitored the decline of the hexacyanoferrate (III) peaks as a function of time of the absorbance band at ≈420 nm at pH 2.0 and pH 5.5 of aqueous colloidal solutions (Figure 5). f5

The UV−vis absorbance spectra of the tested reaction colloidal solutions showed a distinct maximum at 300 nm (∼33,333 cm^{-1}) with a shoulder at 320 nm (∼31,250 cm^{-1}) and a peak at 420 nm (∼23,810 cm^{-1}). The first absorption band can be assigned to the $^2T_{2g}$ electronic transitions of ferrocyanide ion complexes with spin-allowed d → d transitions and its shoulder is indicative for the deprotonated nitrogen end of cyanide as a result of the destabilized T_{2g} level.

In aqueous solution of ibuprofen-Fe_3O_4-GO nanospheres at pH 2.0, the intensity of the analytical peak at 420 nm decreased during the first 15 min of reaction with the development of a broad band near 710 nm (Figure 5a). In the next 30 min of reaction, the intensity of the analytical band

https://doi.org/10.1021/acsanm.3c05399
ACS Appl. Nano Mater. XXXX, XXX, XXX−XXX

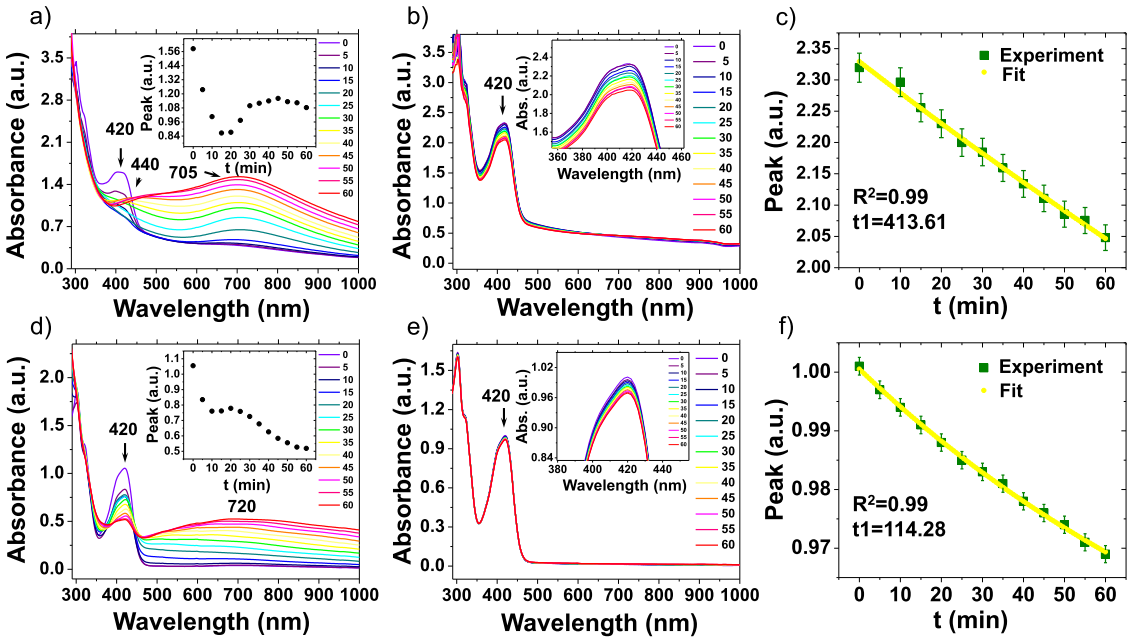

Figure 5. UV−vis absorbance spectra of aqueous solutions of 200 μL of 0.01 M $Fe(CN)_6^{3-}$ and 200 μL of 0.1 M $S_2O_3^{2-}$ with 600 μL of ibuprofen-Fe_3O_4-GO nanospheres at (a) pH 2.0 and (b) pH 5.5 with a local zoom-in peak near 420 nm, and pristine ibuprofen NPs at (d) pH 2.0 and (e) pH 5.5 with a zoom-in peak near 420 nm during 60 min of reaction are shown. Inset plots show the time-dependence evolution of the peak intensity at 420 nm. Plots in (c) and (f) show the experimental data of the peak intensity decay (at 420 nm) after being fitted to the exponential decay function with Pearson's correlation coefficient R^2 = 0.99 and the decay factor $t1$ of ibuprofen-Fe_3O_4-GO nanospheres and pristine ibuprofen NPs.

increased with a spectral shift at 440 nm and reached the plateau under the overlap of a new broad band with the increased continuum (Figure 5a, inset). After an additional 15 min of reaction, the intensity of the analytical band slightly decreased during the growth of a new broad band, which showed a spectral shift at 705 nm. The decrease of the analytical peak at 420 nm is caused by the electron transfer reaction between $Fe(CN)_6^{3-}$ and $S_2O_3^{2-}$ as a result of oxidation of thiosulfate ions. The band diminishing at 420 nm after 15 min demonstrates that $Fe(CN)_6^{3-}$ had fully reacted with $S_2O_3^{2-}$. The following increase of this absorbance band during the next 30 min of reaction can be associated with the formation of different protonated species such as $HFe(CN)_6^{2-}$, $H_2Fe(CN)_6^{-}$ or $H_3Fe(CN)_6$, which is indicative of higher H^+ concentration in aqueous solution. Among these protonated species the active form of oxidant was found to be $HFe(CN)_6^{2-}$ which leads to the reaction products such as hexacyanoferrate(II) and $S_2O_3^{-}$. These changes of the analytical absorbance band are accompanied by the spectral shift at 440 nm and increase of the broadband near 705 nm, indicating mixed charge transfer and ligand field transitions of protonated Fe(II) complexes of ibuprofen in the close proximity of N and phenyl rings.

In contrast, in aqueous solution of ibuprofen-Fe_3O_4-GO nanospheres at pH 5.5, the absorbance peak at 420 nm does not shift during 60 min of reaction, but its intensity decreases following the exponential decay function $y = 0.24 + 2.09e^{(-x/t1)}$ at a rate $t1$ = 413.6 (Figure 5b,c).

UV−vis absorbance spectra of pristine ibuprofen NPs at pH 2.0 show the analytical peak at 420 nm without spectral shift, but with the retarded decay of intensity during 60 min of reaction, demonstrating the electron transfer between $Fe(CN)_6^{3-}$ and $S_2O_3^{2-}$ without enhanced protonation process (Figure 4d). Such a retarded decay is accompanied by a broad absorbance band near 720 nm being developed with increased intensity after 60 min of reaction. This band is indicative of the low-energy charge transfer absorbance of increased concentration of partially or fully deprotonated organic iron-CN complexes with phenyl rings. This absorbance band does not shift because alkyl groups are longer than methyl groups at the bridging nitrogen atom and do not shift the metal−ligand charge transfer to lower energy.

At pH 5.5, only the analytical peak at 420 nm appears with the decreased intensity following the exponential decay function $y = 0.92 + 0.08e^{(-x/t1)}$ at a rate $t1$ = 114.3 during 60 min of reaction (Figure 5e,f). The electron transfer rate of pristine ibuprofen NPs ($t1$ = 114.3) is ~3.6 times lower than that of ibuprofen-Fe_3O_4-GO nanospheres ($t1$ = 413.6), indicating that complexed ibuprofen within Fe_3O_4-GO nanoplatform is more active in the electron transfer process at pH 5.5. In this way, we can assume that at low pH ibuprofen in its nonionized state forms complexes with Fe_3O_4-GO structure, resulting in a free iron coordination site and partial activation of iron species in the electron transfer reaction between $Fe(CN)_6^{3-}$ and $S_2O_3^{2-}$. In contrast, pristine ibuprofen NPs act as iron chelators with a closed coordination site, decreasing the iron activity at low pH.

To prove this assumption, let us consider the nature and concentration of positive ionic species on the surface of ibuprofen-Fe_3O_4-GO nanospheres in comparison with free ibuprofen per se by using the mass spectrometry method. In these experiments, ibuprofen-Fe_3O_4-GO nanospheres were prepared by mechanical stirring or ultrasound in order to find out the effect of ultrasound on complexation of ibuprofen with Fe_3O_4-GO nanoplatform. The determined concentrations of positive ions are listed in Table 2 and the representative mass spectra are shown in Figure S5.

The calculated concentration of positive ions was normalized to the highest concentration of H^+. Overall, the mass spectra of free ibuprofen per se show the highest

https://doi.org/10.1021/acsanm.3c05399
ACS Appl. Nano Mater. XXXX, XXX, XXX−XXX

Table 2. Analysis of Concentration of Positive Ionic Species Formed in Free Ibuprofen Per Se and Ibuprofen-Fe_3O_4-GO Nanospheres Determined by the Time-of-Flight Secondary-Ion Mass Spectrometry Method

intensity of positive ionic species, a.u.	intensity of free ibuprofen per se, a.u.	intensity of ibuprofen-Fe_3O_4-GO (mechanical stirring), a.u.	intensity of ibuprofen-Fe_3O_4-GO (ultrasound), a.u.
H^+	61,240	57,102	60,375
CHO_2^+	11,707	478	1732
OH^+	816	144	521
CO^+	2148	633	1795
C_2^+	421	549	2007
FeO^+		214	271
CFe^+		197	843
$COFe^+$		180	672
H^+		57,102	60,375

concentration of H^+, CHO_2^+, OH^+, and CO^+ than of complexed ibuprofen with Fe_3O_4-GO nanoplatform. The excessive formation of cationic species on pristine ibuprofen can result from the second single-electron oxidation followed by the formation of a benzyl cation, acting as the substrate for the generation of final products: alcohol and ether. At the same time, the labile hydroperoxide can be also formed, which produces a mixture of alcohol and ketone as a result of the addition of oxygen to the benzyl radical.

The mass spectra reveal the concentration of C_2^+ ions being increased by ∼4.8 in ultrasonically formed ibuprofen-Fe_3O_4-GO nanospheres in comparison with pristine ibuprofen, which can be caused by the increased number of complexed ibuprofen molecules in the use of ultrasound. Similarly, the concentration of C_2^+ ions of ibuprofen-Fe_3O_4-GO prepared under mechanical stirring was higher by ∼3.7, indicating that complexation of ibuprofen molecules also takes place under mechanical agitation, but is less efficient than ultrasound. The intensity of detected ionic species such as FeO^+, CFe^+, and $COFe^+$ was also higher by ∼1.3, ∼4.3, and ∼3.7 in ibuprofen-Fe_3O_4-GO nanospheres being formed by ultrasound than under silent conditions, indicating the profound effect of sonochemical reactions on the complexation of ibuprofen with the Fe_3O_4-GO nanoplatform and iron-complexation.

However, the concentration of CHO_2^+, OH^+, and CO^+ is the highest in pristine ibuprofen and the lowest is in ibuprofen-Fe_3O_4-GO nanospheres being formed under silent conditions. We can estimate that ≈14.8% more CHO_2^+ ions are present in ibuprofen-Fe_3O_4-GO nanospheres being formed with ultrasound than without it (≈4.1%) in comparison with free ibuprofen per se. In a similar comparison, the amounts of more OH^+ ions are ≈17.7% (silent) and ≈63.9% (ultrasound), and of more CO^+ are ≈29.5% (silent) and ≈83.6% (ultrasound) in ibuprofen-Fe_3O_4-GO nanospheres than in free ibuprofen per se, demonstrating the important role of CO bonds, COOH and OH groups in the complexation of ibuprofen with Fe_3O_4-GO nanoplatform, which is enhanced by ultrasound.

The ameliorated concentration of FeO^+, CFe^+, and $COFe^+$ on the surface of ibuprofen-Fe_3O_4-GO nanospheres confirms our suggestions derived from the UV−vis absorbance results that ibuprofen forms complexes with mixed charge transfer and increased ligand field transitions of protonated Fe(II) complexes of this drug molecules in the close proximity of N and phenyl rings. In addition, these findings also support the data of CV measurements, which point out to the enhanced $^{\cdot}OH$ radical scavenging ability of ultrasonically formed ibuprofen-Fe_3O_4-GO in contrast to pristine ibuprofen due to increased concentration of inactive protonated Fe(II) centers in Fe−O, C−Fe and CO-Fe bonds (FeO^+, CFe^+ and $COFe^+$) of complexed drug molecules and increased concentration of CHO_2^+, OH^+ and CO^+ ions.

The increased concentration of inactive protonated Fe(II) centers could limit the accessibility of H_2O_2 to the iron, which is related to the number of ligation sites occupied by the chelator. The increased number of protonated ionic species including H^+ on the surface of ibuprofen-Fe_3O_4-GO nanospheres can alter the electro-Fenton mechanism so that little $^{\cdot}OH$ radicals are produced. In this way, the $^{\cdot}OH$ radical scavenging mechanism of ibuprofen-Fe_3O_4-GO is similar to the action of previously reported Fe_3O_4-rGO-SA NPs (salicylic acid complexed with rGO-Fe_3O_4) because both types of NPs act as redox deactivators of iron centers and increase H^+ generation, resulting in efficient diminishing of $^{\cdot}OH$ radicals. However, in contrast to SA-rGO-Fe_3O_4, ibuprofen-Fe_3O_4-GO nanospheres do not require addition of ascorbic acid and still exhibit antioxidant efficiency that is ∼23.5 times higher than that of pristine ibuprofen and ∼161.2 times higher activity than ibuprofen NPs.

4. CONCLUSIONS

We have developed a feasible ultrasonic method (20 kHz) for in situ complexation of pristine ibuprofen molecules at the contact with preformed Fe_3O_4-GO nanoplatform by applying the "solvent:antisolvent" (ethanol:aqueous fluids) acoustic emulsification mechanism. As a result, ibuprofen-Fe_3O_4-GO nanospheres with a core−shell structure and an average size of ∼51 nm were prepared. The ultrasonic complexation of pristine ibuprofen with the Fe_3O_4-GO nanoplatform occurs via the H-bond formation with the drug side chains (CH, CH_2, and CH_3) and C−O−H interaction of carboxylic groups with Fe−O bonds.

Ibuprofen-Fe_3O_4-GO nanospheres are efficient $^{\cdot}OH$ scavengers in the electro-Fenton process with ∼23.5 times higher diminishing rate efficiency than pristine ibuprofen and ∼161.2 times higher activity than ibuprofen NPs. This pronounced antioxidant efficiency of ibuprofen-Fe_3O_4-GO is due to the increased concentration of inactive protonated Fe(II) centers in Fe−O, C−Fe, and CO−Fe bonds (FeO^+, CFe^+, and $COFe^+$) of complexed drug molecules and increased concentration of CHO_2^+, OH^+, and CO^+ ions on the surface of nanospheres. As a result, ibuprofen-Fe_3O_4-GO can limit the accessibility of H_2O_2 to the iron and deactivate it and substantially decrease the production of $^{\cdot}OH$ radicals. This effect is enhanced via the neutralization of $^{\cdot}OH$ radicals with various cationic active species present on the surface of ibuprofen-Fe_3O_4-GO nanospheres.

This new knowledge substantially improves the understanding of iron inactivation and free radical scavenging activity as two basic mechanisms of the ibuprofen antioxidant function that can be modulated by Fe_3O_4-GO at the nanoscale. The demonstrated method discloses the conditions of modulation and enhanced antioxidant efficiency of ibuprofen and can be potentially applied to other drugs.

https://doi.org/10.1021/acsanm.3c05399
ACS Appl. Nano Mater. XXXX, XXX, XXX−XXX

■ ASSOCIATED CONTENT

Supporting Information

The Supporting Information is available free of charge at https://pubs.acs.org/doi/10.1021/acsanm.3c05399.

EDX spectra and SEM images of GO after first and second oxidation protocols; SEM image and EDX spectrum of the synthesized Fe_3O_4-GO nanoplatform; TEM images of ibuprofen-Fe_3O_4-GO and pristine ibuprofen nanoparticles; Raman spectrum of bulk magnetite material; analysis of experimental FTIR transmittance spectra of pristine ibuprofen, GO, Fe_3O_4-GO nanoplatform, and ibuprofen-Fe_3O_4-GO nanospheres; analysis of experimental XRD powder diffractograms of free ibuprofen per se; optical phase contrast microscopy images of pristine ibuprofen nanoparticles after 24 h of aging in a mother solution; and TOF SIMS mass spectra of free ibuprofen per se and ibuprofen-Fe_3O_4-GO nanospheres formed by mechanical stirring or ultrasound (PDF)

■ AUTHOR INFORMATION

Corresponding Author

Darya Radziuk − *Laboratory of Integrated Micro- and Nanosystems, Belarusian State University of Informatics and Radioelectronics, 220013 Minsk, Republic of Belarus;* orcid.org/0000-0003-1409-5357; Email: radziuk@bsuir.by

Authors

Aleksey Drinevskyi − *Laboratory of Integrated Micro- and Nanosystems, Belarusian State University of Informatics and Radioelectronics, 220013 Minsk, Republic of Belarus*

Evgenij Zelkovskyi − *Laboratory of Integrated Micro- and Nanosystems, Belarusian State University of Informatics and Radioelectronics, 220013 Minsk, Republic of Belarus*

Vladimir Labunov − *Laboratory of Integrated Micro- and Nanosystems, Belarusian State University of Informatics and Radioelectronics, 220013 Minsk, Republic of Belarus*

Complete contact information is available at: https://pubs.acs.org/10.1021/acsanm.3c05399

Author Contributions

The manuscript was written through contributions of all authors. All authors have given approval to the final version of the manuscript.

Funding

This work was supported by the Belarusian Republican Foundation for Fundamental Research grant SCIENTIST No. F22Y-007 and Belarusian Ministry of Education Research grant No. 21-3067 1.17.

Notes

The authors declare no competing financial interest.

■ ACKNOWLEDGMENTS

We acknowledge D. Zhigulin (Scientific-Technical Center "Belmicrosystems", Minsk) for the analysis and helpful discussion in the use of time-of-flight secondary-ion mass spectrometry, Dr. K.V. Skrotskaya for insightful TEM analysis (Belarusian State University), Prof. V.P. Bondarenko for access to Metrohm Autolab potentiostat/galvanostat instrument, and T. Rysalskaya for assistance in the synthesis of graphene oxide (Belarusian State University of Informatics and Radioelectronics).

■ REFERENCES

(1) Mazaleuskaya, L. L.; Theken, K. N.; Gong, L.; Thorn, C. F.; FitzGerald, G. A.; Altman, R. B.; Klein, T. E. PharmGKB summary: ibuprofen pathways. *Pharmacogenet Genomics* **2015**, *25*, 96−106.

(2) Petrat, F.; de Groot, H.; Sustmann, R.; Rauen, U. The chelatable iron pool in living cells: a methodically defined quantity. *Biol. Chem.* **2002**, *383*, 489−502.

(3) Kehrer, J. P. The Haber-Weiss reaction and mechanisms of toxicity. *Toxicology* **2000**, *149*, 43−50.

(4) Poprac, P.; Jomova, K.; Simunkova, M.; Kollar, V.; Rhodes, C. J.; Valko, M. Targeting free radicals in oxidative stress-related human diseases. *Trends Pharmacol. Sci.* **2017**, *38*, 592−607.

(5) Naruszewicz, M.; Zapolski-Downar, A.; Markiewski, M.; Bukowska, H.; Millo, B. Ibuprofen inhibits adhesiveness of monocytes to endothelium and reduces cellular oxidative stress in smokers and non-smokers. *Eur. J. Clin. Invest.* **2000**, *30*, 1002−1010.

(6) Zapolska-Downar, D.; Naruszewicz, M. A pleiotropic anti-atherogenic action of ibuprofen. *Med. Sci. Monit.* **2001**, *7*, 837−841.

(7) Zapolska-Downar, D.; Zapolski-Downar, A.; Bukowska, H.; Gałka, H.; Naruszewicz, M. Ibuprofen protects low density lipoproteins against oxidative modification. *Life Sci.* **1999**, *65*, 2289−2303.

(8) Cohen, G. The Fenton reaction. In *Handbook of Methods for Oxygen Radical Research*; Greenwald, R. A., Ed.; CRC Press, Inc.: Boca Raton, FL, 1985; pp 55−69.

(9) Orhan, H.; Şahin, G. In vitro effects of NSAIDS and paracetamol on oxidative stress-related parameters of human erythrocytes. *Exp. Toxic Pathol.* **2001**, *53*, 133−140.

(10) Hamburger, S. A.; McCay, P. B. Spin trapping of ibuprofen radicals: evidence that ibuprofen is a hydroxyl radical scavenger. *Free Rod. Reg. Comms.* **1990**, *9*, 337−342.

(11) Van Antwerpen, P.; Nève, J. In vitro comparative assessment of the scavenging activity against three reactive oxygen species of non-steroidal anti-inflammatory drugs from the oxicam and sulfoanilide families. *Eur. J. Pharmacol.* **2004**, *496*, 55−61.

(12) Kennedy, T. P.; Rao, N. V.; Noah, W.; Michael, J. R.; Jafri, M. H.; Gurtner, G. H.; Hoidal, J. R. Ibuprofen prevents oxidant lung injury and in vitro lipid peroxidation by chelating iron. *J. Clin. Invest.* **1990**, *86*, 1565−1573.

(13) Albert, A. Chemical aspects of selective toxicity. *Nature* **1958**, *182* (4633), 421−422.

(14) Banti, C. N.; Hadjikakou, S. K. Non-steroidal anti-inflammatory drugs (NSAIDs) in metal complexes and their effect at the cellular level. *EurJIC* **2016**, *2016*, 3048−3071.

(15) Liu, Q.; Du, K.; Liu, M.; Lv, R.; Sun, B.; Cao, D.; He, N.; Wang, Z. Sulfosalicylic acid/Fe^{3+} based nanoscale coordination polymers for effective cancer therapy by the Fenton reaction: an inspiration for understanding the role of aspirin in the prevention of cancer. *Biomater. Sci.* **2019**, *7*, 5482−5491.

(16) Kataoka, M. A.; Tonooka, K.; Ando, T.; Imai, K.; Aimoto, T. Hydroxyl radical scavenging activity of nonsteroidal anti-inflammatory drugs. *Free Radic. Res.* **1997**, *27*, 419−427.

(17) Mikhnavets, L.; Abashkin, V.; Khamitsevich, H.; Shcharbin, D.; Burko, A.; Krekoten, N.; Radziuk, D. Ultrasonic formation of Fe_3O_4 reduced graphene oxide-salicylic acid nanoparticles with switchable antioxidant function. *ACS Biomater. Sci. Eng.* **2022**, *8*, 1181−1192.

(18) Alegret, N.; Criado, A.; Prato, M. Recent advances of graphene-based hybrids with magnetic nanoparticles for biomedical applications. *Curr. Med. Chem.* **2017**, *24*, 529−536.

(19) Zhang, Y.; Zhang, Y.; Yang, Z.; Fan, Y.; Chen, M.; Zhao, M.; Dai, B.; Zheng, L.; Zhang, D. Cytotoxicity effect of iron oxide (Fe_3O_4)/graphene oxide (GO) nanosheets in cultured HBE cells. *Front Chem.* **2022**, *10*, No. 888033.

(20) Wang, Q.; Zhang, X.; Huang, L.; Zhang, Z.; Dong, S. One-pot synthesis of Fe_3O_4 nanoparticle-loaded 3D porous graphene nano-

composites with enhanced nanozyme activity for glucose detection. *ACS Appl. Mater. Interfaces* **2017**, *9*, 7465−7471.
(21) Yang, X.; Zhang, X.; Ma, Y.; Huang, Y.; Wang, Y.; Chen, Y. Superparamagnetic graphene oxide−Fe_3O_4 nanoparticles hybrid for controlled targeted drug carriers. *J. Mater. Chem.* **2009**, *19*, 2710−2714.
(22) Wang, G.; Chen, G.; Wei, Z.; Dong, X.; Qi, M. Multifunctional Fe_3O_4/graphene oxide nanocomposites for magnetic resonance imaging and drug delivery. *Mater. Chem. Phys.* **2013**, *141*, 997−1004.
(23) Shen, J.-M.; Gao, F.-Y.; Guan, L.-P.; Su, W.; Yang, Y.-J.; Lia, Q.-R.; Jin, Z.-C. Graphene oxide−Fe_3O_4 nanocomposite for combination of dual-drug chemotherapy with photothermal therapy. *RSC Adv.* **2014**, *4*, 18473−18484.
(24) Fiadosenka, U.; Matsukovich, A.; Tabulina, L.; Labunov, V.; Radziuk, D. The properties of the sonochemically functionalized nonsteroidal anti-inflammatory drug ketorolac in Fe_3O_4-graphene oxide nanocomposite. *New J. Chem.* **2019**, *41*, 16118−16122.
(25) Tkach, A.; Fiadosenka, U.; Burko, A.; Bandarenka, H. V.; Matsukovich, A.; Krekoten, N.; Tabulina, L.; Labunov, V.; Radziuk, D. Polyvinyl alcohol enhances acetylation of ascorbic acid in superparamagnetic-graphene oxide nanoparticles ultrasonically complexed with acetylsalicylic acid. *ACS Appl. Polym. Mater.* **2020**, *2*, 3663−3673.
(26) Nel, J.; Siniscalco, D.; Hognon, C.; Bouché, M.; Touche, N.; Brunner, E.; Gros, P. C.; Monari, A.; Grandemange, S.; Francius, G. Structural and morphological changes of breast cancer cells induced by iron(II) complexes. *Nanoscale* **2022**, *14*, 2735−2749.
(27) Meier-Menches, S. M.; Casini, A. Design strategies and medicinal applications of metal-peptidic bioconjugates. *Bioconjugate Chem.* **2020**, *31*, 1279−1288.
(28) Zegers, J.; Peters, M.; Albada, B. DNA G-quadruplex-stabilizing metal complexes as anticancer drugs. *JBIC* **2023**, *28*, 117−138.
(29) Xue, X.; Qian, C.; Tao, Q.; Dai, Y.; Lv, M.; Dong, J.; Su, Z.; Qian, Y.; Zhao, J.; Liu, H.-K.; Guo, Z. Using bio-orthogonally catalyzed lethality strategy to generate mitochondria-targeting anti-tumor metallodrugs in vitro and in vivo. *Natl. Sci. Rev.* **2021**, *8*, No. nwaa286, DOI: 10.1093/nsr/nwaa286.
(30) Wang, H.; Zhou, Y.; Xu, X.; Li, H.; Sun, H. Metalloproteomics in conjunction with other omics for uncovering the mechanism of action of metallodrugs: mechanism-driven new therapy development. *Curr. Opin. Chem. Biol.* **2020**, *55*, 171−179.
(31) Radziuk, D.; Mikhnavets, L.; Vorokhta, M.; Matolín, V.; Tabulina, L.; Labunov, V. Sonochemical formation of copper/iron-modified graphene oxide nanocomposites for ketorolac delivery. *Chem. − Eur. J.* **2019**, *25*, 6233−6245.
(32) Suslick, K. S. The dawn of ultrasonics and the palace of science. *Acoust. Today* **2019**, *15*, 38−46.
(33) Suslick, K. S. *Sonochemistry. Science* **1990**, *247*, 1439−1445.
(34) Weissler, A. Formation of hydrogen peroxide by ultrasonic waves: free radicals. *J. Am. Chem. Soc.* **1959**, *81*, 1077−1081.
(35) Shimanovich, U.; Gedanken, A. Nanotechnology solutions to restore antibiotic activity. *J. Mater. Chem. B* **2016**, *4*, 824−833.
(36) Zeiger, B. W.; Suslick, K. S. Sonofragmentation of molecular crystals. *J. Am. Chem. Soc.* **2011**, *133*, 14530−14533.
(37) Kim, H. N.; Suslick, K. S. Sonofragmentation of organic molecular crystals vs strength of materials. *J. Org. Chem.* **2021**, *86*, 13997−14003.
(38) Grinberg, O.; Shimanovich, U.; Gedanken, A. Encapsulating bioactive materials in sonochemically produced micro-and nano-spheres. *J. Mater. Chem. B* **2013**, *1*, 595−605.
(39) Mukh-Qasem, R. A.; Gedanken, A. Sonochemical synthesis of stable hydrosol of Fe_3O_4 nanoparticles. *J. Colloid Interface Sci.* **2005**, *284*, 489−494.
(40) Zhu, S.; Guo, J.; Dong, J.; Cui, Z.; Lu, T.; Zhu, C.; Zhang, D.; Mac, J. Sonochemical fabrication of Fe_3O_4 nanoparticles on reduced graphene oxide for biosensors. *Ultrason. Sonochem.* **2013**, *20*, 872−880.
(41) Niu, G.; Yousefi, B.; Qujeq, D.; Marjani, A.; Asadi, J.; Wang, Z.; Mir, S. M. Melatonin and doxorubicin co-delivered via a functionalized graphene-dendrimeric system enhances apoptosis of osteosarcoma cells. *Mater. Sci. Eng. C Mater. Biol. Appl.* **2021**, *119*, No. 111554.
(42) Wang, Z.; Zhou, C.; Xia, J.; Via, B.; Xia, Y.; Zhang, F.; Li, Y.; Xia, L. Fabrication and characterization of a triple functionalization of graphene oxide with Fe_3O_4, folic acid and doxorubicin as dual-targeted drug nanocarrier. *Colloids Surf. B: Biointerfaces* **2013**, *106*, 60−65.
(43) Li, N.; Chen, J.; Shi, Y.-P. Magnetic polyethyleneimine functionalized reduced graphene oxide as a novel magnetic sorbent for the separation of polar non-steroidal anti-inflammatory drugs in waters. *Talanta* **2019**, *191*, 526−534.
(44) Li, G.; Deng, R.; Peng, G.; Yang, C.; He, Q.; Lu, Y.; Shi, H. Magnetic solid-phase extraction for the analysis of bisphenol A, naproxen and triclosan in wastewater samples. *Water Sci. Technol.* **2018**, *77*, 2220−2227.
(45) Yuvali, D.; Narin, I.; Soylak, M.; Yilmaz, E. Green synthesis of magnetic carbon nanodot/graphene oxide hybrid material (Fe_3O_4@C-nanodot@GO) for magnetic solid phase extraction of ibuprofen in human blood samples prior to HPLC-DAD determination. *J. Pharm. Biomed. Anal.* **2020**, *179*, No. 113001.
(46) Cao, L.; Jiang, Y.; Chen, Z. Hollow Fe_3O_4/graphene oxide nanocomposites as novel rapamycin carrier: formulation optimization and in vitro characterization. *J. Nanosci. Nanotechnol.* **2018**, *18*, 3067−3076.
(47) Asgharinezhad, A. A.; Ebrahimzadeh, H. Poly(2-amino-benzothiazole)-coated graphene oxide/magnetite nanoparticles composite as an efficient sorbent for determination of non-steroidal anti-inflammatory drugs in urine sample. *J. Chromatogr. A* **2016**, *1435*, 18−29.
(48) Jacintho, G. V. M.; Brolo, A. G.; Corio, P.; Suarez, P. A. Z.; Rubim, J. C. Structural investigation of MFe_2O_4 (M = Fe, Co) magnetic fluids. *J. Phys. Chem. C* **2009**, *113*, 7684−7691.
(49) Knight, D. S.; White, W. B. Characterization of diamond films by Raman spectroscopy. *J. Mater. Res.* **1989**, *4*, 385−393.
(50) Ferrari, A. C.; Robertson, J. Interpretation of Raman spectra of disordered and amorphous carbon. *Phys. Rev. B* **2000**, *61*, 14095−14107.
(51) Jubert, A.; Legarto, M. L.; Massa, N. E.; Tévez, L. L.; Okulik, N. B. Vibrational and theoretical studies of non-steroidal anti-inflammatory drugs Ibuprofen [2-(4-isobutylphenyl)propionic acid]; Naproxen [6-methoxy-α-methyl-2-naphthalene acetic acid] and Tolmetin acids [1-methyl-5-(4-methylbenzoyl)-1H-pyrrole-2-acetic acid]. *J. Mol. Struct.* **2006**, *783*, 34−51.
(52) Gera, T.; Nagy, E.; Smausz, T.; Budai, J.; Ajtai, T.; Kun-Szabó, F.; Homik, Z.; Kopniczky, J.; Bozóki, Z.; Szabó-Révész, P.; Ambrus, R.; Hopp, B. Application of pulsed laser ablation (PLA) for the size reduction of non-steroidal anti-inflammatory drugs (NSAIDs). *Sci. Rep.* **2020**, *10*, 15806.
(53) Soler, M. A. G.; Qu, F. Raman spectroscopy of iron oxide nanoparticles. In Challa S. S. R., Kumar, Ed.; *Raman Spectroscopy for Nanomaterials Characterization*; Springer-Verlag: Berlin Heidelberg, 2012; p 404.
(54) Solbrig, R. M.; Duff, L. L.; Shriver, D. F.; Klotz, I. M. Raman and infrared spectroscopy of the oxo-bridged iron(III) complex, $[Cl_3Fe\text{-}O\text{-}FeCl_3]^{-2}$ as a spectroscopic model for the oxo bridge in hemerythrin and ribonucleotide reductase. *J. Inorg. Biochem.* **1982**, *17*, 69−74.
(55) Verble, J. L. Temperature-dependent light-scattering studies of the Verwey transition and electronic disorder in magnetite. *Phys. Rev. B* **1974**, *9*, 5236.
(56) Chamritski, I.; Burns, G. Infrared- and Raman-active phonons of magnetite, maghemite, and hematite, a computer simulation and spectroscopic study. *J. Phys. Chem. B* **2005**, *109*, 4965−4968.
(57) Sehested, K.; Corfitzen, H.; Christensen, H. C.; Hart, E. J. Rates of reaction of oxygen(1-) ions, hydroxyl radicals, and atomic hydrogen with methylated benzenes in aqueous solution. Optical spectra of radicals. *J. Phys. Chem.* **1975**, *79*, 310−315.

https://doi.org/10.1021/acsanm.3c05399
ACS Appl. Nano Mater. XXXX, XXX, XXX−XXX

(58) Musa, K. A. K.; Eriksson, L. A. Theoretical study of ibuprofen phototoxicity. *J. Phys. Chem. B* **2007**, *111*, 13345−13352.
(59) Illés, E.; Takács, E.; Dombi, A.; Gajda-Schrantz, K.; Rácz, G.; Gonter, K.; Wojnárovits, L. Hydroxyl radical induced degradation of ibuprofen. *Sci. Total Environ.* **2013**, *447*, 286−292.
(60) Jasim, D. A.; Lozano, N.; Kostarelos, K. Synthesis of few-layered, high-purity graphene oxide sheets from different graphite sources for biology. *2D Mater.* **2016**, *3*, No. 014006.
(61) Mürbe, J.; Rechtenbach, A.; Töpfer, J. Synthesis and physical characterization of magnetite nanoparticles for biomedical application. *Mater. Chem. Phys.* **2008**, *110*, 426−433.
(62) Dimiev, A. M.; Alemany, L. B.; Tour, J. M. Graphene oxide. Origin of acidity, its instability in water, and a new dynamic structural model. *ACS Nano* **2013**, *7*, 576−658.
(63) Dimiev, A. M.; Ceriotti, G.; Behabtu, N.; Zakhidov, D.; Pasquali, M.; Saito, R.; Tour, J. M. Direct real - time monitoring of stage transitions in graphite intercalation compounds. *ACS Nano* **2013**, *7*, 2773−2780.
(64) Rozel, P.; Radziuk, D.; Mikhnavets, L.; Khokhlov, E.; Shiripov, V.; Matolínová, I.; Matolín, V.; Basaev, A.; Kargin, N.; Labunov, V. Properties of nitrogen/silicon doped vertically oriented graphene produced by ICP CVD roll-to-roll technology. *Coatings* **2019**, *9*, 60.
(65) Chen, S.; Xi, H.; Henry, R. F.; Marsden, I.; Zhang, G. G. Z. Chiral co-crystal solid solution: structures, melting point phase diagram, and chiral enrichment of (ibuprofen)2(4,4-dipyridyl). *CrystEngComm* **2010**, *12*, 1485−1493.
(66) Rossi, P.; Macedi, E.; Paoli, P.; Bernazzani, L.; Carignani, E.; Borsacchi, S.; Geppi, M. Solid-solid transition between hydrated racemic compound and anhydrous conglomerate in Na-ibuprofen: A combined X-ray diffraction. Solid-state NMR, Calorimetric, and computational study. *Cryst. Growth Des.* **2014**, *14*, 2441−2452.
(67) Nakagiri, N.; Manghnani, M. H.; Ming, L. C.; Kimura, S. Crystal structure of magnetite under pressure. *Phys. Chem. Miner.* **1986**, *13*, 238−244.
(68) Gatta, G. D.; Kantor, I.; Ballaran, T. B.; Dubrovinsky, L.; McCammon, C. Effect of non-hydrostatic conditions on the elastic behaviour of magnetite: an in situ single-crystal X-ray diffraction study. *Phys. Chem. Miner.* **2007**, *34*, 627−635.
(69) Ostrowska, K.; Kropidłowska, M.; Katrusiak, A. High-pressure crystallization and structural transformations in compressed R. *S*-*ibuprofen. Cryst. Growth Des.* **2015**, *15*, 1512−1517.
(70) Lima, A. B.; Faria, E. O.; Montes, R. H. O.; Cunha, R. R.; Richter, E. M.; Munoz, R. A. A.; dos Santos, W. T. P. Electrochemical oxidation of ibuprofen and its voltammetric determination at a boron-doped diamond electrode. *Electroanalysis* **2013**, *25*, 1585−1588.

https://doi.org/10.1021/acsanm.3c05399
ACS Appl. Nano Mater. XXXX, XXX, XXX−XXX